Antiproton production in $p+A$ collisions at 12.3 and 17.5 GeV/c

I. Chemakin,[1] V. Cianciolo,[2,3] B. A. Cole,[1] R. Fernow,[4] A. Frawley,[5] M. Gilkes,[6] S. Gushue,[4] E. Hartouni,[2] H. Hiejima,[1]
M. Justice,[7] J. H. Kang,[8] D. Keane,[7] H. Kirk,[4] M. Kreisler,[2] N. Maeda,[5] R. L. McGrath,[6] S. Mioduszewski,[4,9]
D. Morrison,[9] M. Moulson,[1] N. Namboodiri,[2] G. Rai,[10] K. Read,[9] L. Remsberg,[4] M. Rosati,[4,11] Y. Shin,[8] R. Soltz,[2]
S. Sorensen,[9] J. Thomas,[2,4,10] Y. Torun,[4,6,12] D. Winter,[1] X. Yang,[1] W. A. Zajc,[1] and Y. Zhang[1]

[1]*Columbia University, New York, New York 10027
and Nevis Laboratories, Irvington, New York 10533*
[2]*Lawrence Livermore National Laboratory, Livermore, California 94550*
[3]*Oak Ridge National Laboratory, Oak Ridge, Tennessee 37831*
[4]*Brookhaven National Laboratory, Upton, New York 11973*
[5]*Florida State University, Tallahasee, Florida 32306*
[6]*State University of New York at Stony Brook, Stony Brook, New York 11794*
[7]*Kent State University, Kent, Ohio 44242*
[8]*Yonsei University, IPAP, Seoul 120-749, Korea*
[9]*University of Tennessee, Knoxville, Tennessee 37996*
[10]*Ernest O. Lawrence Berkeley National Laboratory, Berkeley, California 94720*
[11]*Iowa State University, Ames, Iowa 50010*
[12]*Illinois Institute of Technology, Chicago, Illinois 60616*
(Received 18 July 2001; published 20 November 2001)

Inclusive and semi-inclusive measurements are presented for antiproton ($\bar{p}$) production in proton-nucleus collisions at the Alternating Gradient Synchrotron (AGS). The inclusive yields per event increase strongly with increasing beam energy and decrease slightly with increasing target mass. The $\bar{p}$ yield in 17.5 GeV/c p + Au collisions decreases with grey track multiplicity, N_g, for $N_g>0$, consistent with annihilation within the target nucleus. The relationship between N_g and the number of scatterings of the proton in the nucleus is used to estimate the $\bar{p}$ annihilation cross section in the nuclear medium. The resulting cross section is at least a factor of 5 smaller than the free $\bar{p}$-p annihilation cross section when assuming a small or negligible formation time. Only with a long formation time can the data be described with the free $\bar{p}$-p annihilation cross section.

Antiprotons are a topic of great interest in relativistic heavy ion physics [1–5] because enhanced production may result from the formation of the quark gluon plasma (QGP) [6] and because antiprotons may provide an experimental measure of the baryon density of matter produced in $A+A$ collisions due to the large $\bar{p}$-p annihilation cross section [7]. Comparisons of antiproton production in E802 [8] and E878 [9] with cascade models show that, in fact, more antiprotons are produced in these collisions than would be expected from ordinary hadronic production and the effects of final-state absorption. However, the same models have shown that these larger $\bar{p}$ yields could result from increased production and/or decreased absorption. One proposed mechanism for increased production of $\bar{p}$ is the multiple scattering of the incident baryons [10]. Several mechanisms for decreased absorption have been proposed including a finite $\bar{p}$ formation time, "shielding" of the absorption process [11] (ARC), and a time delay due to the formation of a p-$\bar{p}$ quasi-bound-state [12,13] (RQMD). Proton-nucleus collisions provide a valuable tool for disentangling these competing effects and elucidating the dynamics of antiproton production and absorption in a nuclear environment because the density of absorbers (nucleons) in the nucleus is well understood. In particular, at energies close to the antiproton production threshold, it is expected that most antiprotons will be pro-

duced from the first scattering of the proton in the nucleus. The remaining thickness of the nucleus may then simply act as an absorber. Previous measurements of $\bar{p}$ production in $p+A$ collisions have been hindered by poor statistics and the fact that most $p+A$ measurements are inclusive. Antiproton yields presented here are shown first inclusively, comparing different beam energies and targets, and then as a function of the number of scatterings of the projectile proton in the nucleus. We focus on our semi-inclusive measurement to address questions about the first-collision model and in-medium modifications to the annihilation cross section.

E910 is a $p+A$ experiment based on a time projection chamber with downstream tracking and Cerenkov (CKOV) and time-of-flight (TOF) detectors. The E910 apparatus has been described in detail elsewhere [14], but here we will again give a brief description of the time-of-flight (TOF) detector, used to identify antiprotons, and the trigger used for this data set. The TOF is located approximately 8 m from the target with an active area of approximately 5×2 m^2. It is made up of 32 scintillating slats with readout at the top and bottom of each slat. Protons can be separated from pions and kaons by more than 2σ up to a momentum of 3.0 GeV/c and by more than 1σ up to 3.5 GeV/c, where the timing resolution for protons is 164 ps. The data presented here were collected with a scintillating fiber trigger. The scintillating fiber was placed approximately 2 cm downstream of the tar-
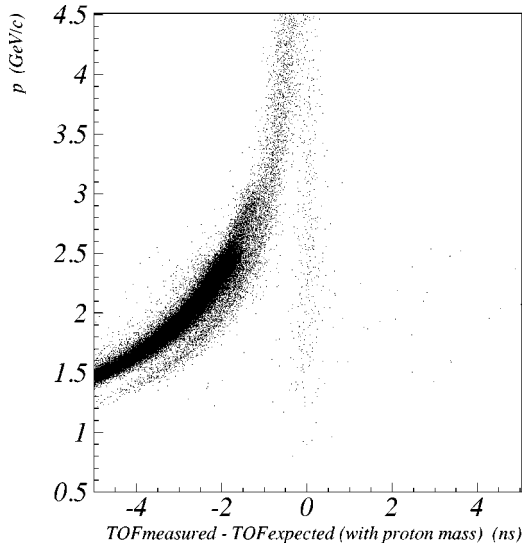
FIG. 1. Total momenta for negative tracks vs difference between measured flight time and expected flight time in ns.

TABLE I. Final (raw) event statistics.

Target	p (GeV/c)	No. min. bias triggers	No. central triggers	No. $\bar{p}$ min. bias	No. $\bar{p}$ central
Au	17.5	2.66×10^6	1.06×10^6	346	93
Au	12.3	1.69×10^6	0.46×10^6	73	6
Cu	12.3	1.26×10^6	0	84	0
Be	12.3	1.41×10^6	0	102	0

get. A minimum bias interaction is defined as an event having two hits in each of the two layers of the scintillating fiber, and a central interaction is an event with a total of 20 or more hits in the fiber. We include only central triggers for which there were greater than 2 ''grey tracks'' in the event, where a grey track is defined as a ''slow'' proton or deuteron. A slow proton has momentum $0.25 < p < 1.2$ GeV/c and a slow deuteron has momentum $0.5 < p < 2.4$ GeV/c.

For track quality, we require at least 10 hits in the time projection chamber (TPC) and that the track originated from the event vertex. Although our primary particle identification for antiprotons comes from time of flight, we additionally use Cerenkov information and ionization energy loss in the TPC to reduce background. We require that the ionization energy loss is within 3σ of the proton dE/dx. In the relativistic rise region, where the pion band separates from the proton, the measured dE/dx must be greater than 1.5σ from the pion dE/dx. We also apply a cut on the Cerenkov analog to digital converter (ADC), which, on average, corresponds to requiring less than 0.35 photoelectrons. The effect of these cuts on the background can be seen in Fig. 1, which will be described later in the text. Quality cuts on the hits on the time-of-flight wall (TOF) include a cut on the difference in horizontal position between a projected track and the center of a hit TOF slat, and a cut on the energy deposited on the TOF slat. We further require the projected track to have at least 5 hits in the three drift chambers located between the TPC and the TOF wall. We determine the efficiencies of these cuts and correct for them in y and p_T. Tracks are matched to the TOF wall with an $90 \pm 5\%$ efficiency. A single correction factor is applied uniformly over y and p_T. The 5% systematic uncertainty in this correction is included in the overall errors of the results.

Figure 1 shows the momentum dependence for negative tracks of the difference between the measured time of flight and the expected time of flight assuming the mass of a proton. The cuts on this distribution are momentum dependent and range from 800 ps for low momentum tracks to 200 ps

for tracks with momenta between 3 and 3.5 GeV/c. A momentum-dependent background of the identified antiprotons is calculated and subtracted, amounting to an overall correction of approximately 5%. The data have been acceptance corrected within our y-p_T coverage and corrected for the efficiencies of our cuts as mentioned above. Our coverage ranges from 10 to 800 MeV/c in p_T and 1 to 2 in units of rapidity. The acceptance is largest at low p_T near rapidities between 1.6 and 2.0. The acceptance is limited in the low y, high p_T region by the spatial coverage of the TOF wall, while the high y region is limited by the upper momentum cut of 3.5 GeV/c. Since a sample of identified protons, using loose TOF criteria, is relatively clean compared to a sample of loosely identified antiprotons, the efficiency of the cuts can be estimated by applying the cuts to the sample of identified protons. The overall calculated efficiency ranges from 60% to 80%, decreasing with increasing p_T. The cut on the difference in horizontal position of the projected track from the TOF hit is most inefficient near the edges of the TOF wall, thus affecting primarily the low y, high p_T region. The particle identification cuts (on dE/dx and the Cerenkov ADC), which reduce the background, affect the efficiency primarily for higher momentum antiprotons (high y, high p_T region). We neglect the inefficiency due to multiple hits in one TOF slat because the slat occupancy is only approximately 3%. Even in central events, where the multiplicities are larger, the slat occupancy is less than 3% because the particles tend to shift back in rapidity and thus out of the acceptance of the TOF wall. The data have also been corrected for trigger biases that are determined by examining beam-triggered events (unbiased events) in two dimensions, the total number of charged particles in the event and the number of grey tracks N_g in the event. Particularly in ''central'' interaction triggered events, but also in ''minimum bias'' interaction triggered events, there is a bias against events with small numbers of charged particles and small N_g. This bias can be determined from beam-triggered events, by comparing the distribution of the number of charged particles and N_g for those beam-triggered events that also passed the conditions for an interaction trigger to the unbiased distribution. We estimate feeddown from antilambdas, by applying the $\bar{p}$ selection cuts to a set of antilambdas identified in the TPC, to be less than 5%. Final (raw) event statistics for each data set are shown in Table I. The data sets analyzed include 17.5 GeV/c momentum $p + $Au collisions, 12.3 GeV/$c$ $p + $Au, 12.3 GeV/$c$ $p + $Cu, and 12.3 GeV/$c$ $p + $Be. The target thicknesses are 4.5%, 3.1%, and 2.0% of the interaction length for Be, Cu, and Au, respectively.
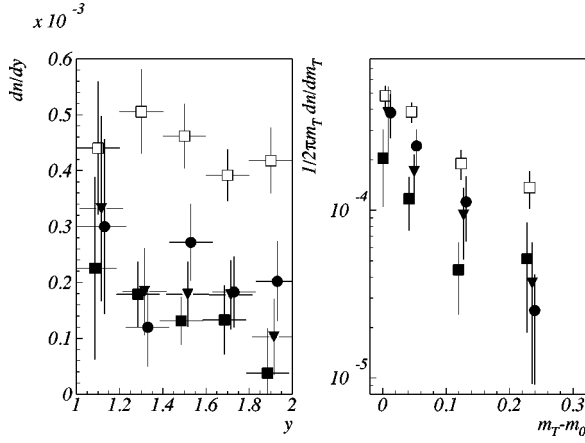
FIG. 2. Target and beam momentum dependence of $p+A$ $\bar{p}$ spectra, (a) dn/dy distributions, (b) m_T distributions, $p+$Be ($\bullet$); $p+$Cu ($\blacktriangledown$); $p+$Au ($\blacksquare$) at 12.3 GeV/c; 17.5 GeV/c $p+$Au ($\square$). The points from different data sets are offset relative to each other in order to distinguish the error bars.
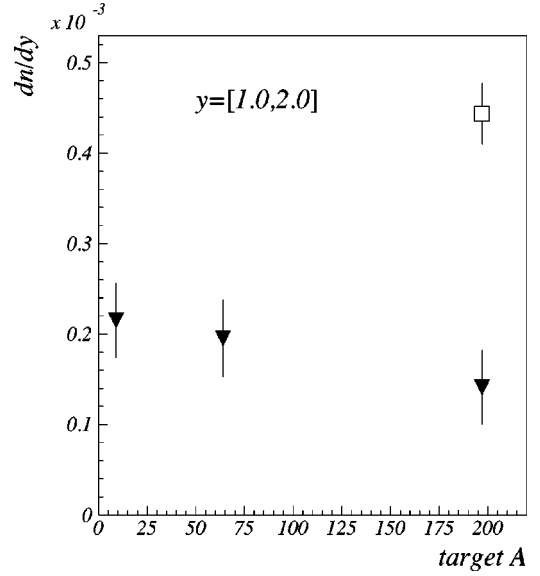

FIG. 3. Target mass dependence of E910 $\bar{p}$ yields summed over $1<y<2$; yields for 12.3 GeV/c beam momentum ($\blacktriangledown$); 17.5 GeV/c ($\square$).

Our measure of centrality is defined by the number of projectile collisions ν, which is derived from the number of grey tracks N_g in an event. Slow protons and deuterons are identified by their measured ionization energy loss in the TPC. The momentum cut on the protons is $0.25<p<1.2$ GeV/c and on the deuterons is $0.5<p<2.4$ GeV/c. For a class of events with a given number of grey tracks N_g, we derive the mean number of collisions. The details of our method to determine $\langle \nu(N_g) \rangle$ are described elsewhere [14].

Antiproton yields for all four data sets are shown in Fig. 2 as a function of rapidity and transverse mass. The beam energy dependence is seen by comparing the two $p+$Au data sets. The yields increase approximately by a factor of 3 from 12.3 to 17.5 GeV/c. The yields for the different target sizes can also be compared in this figure. The transverse mass m_T distribution for each target and beam momentum is fit to the following exponential:

$$\frac{1}{2\pi m_T}\frac{dn}{dm_T} = C_0 e^{-(m_T - m_0)/T}, \tag{1}$$

where C_0 and T are fit parameters. The results of the fits are tabulated in Table II. Due to limited statistics, the errors on the fit parameters are large. However, comparing the inverse slope parameter for the largest data set, 17.5 GeV/c $p+$Au, with that of the 12.3 GeV/c $p+$Be data set shows a significant increase from the smaller target to the larger target. Although the comparison is between two data sets with dif-

TABLE II. Fit parameters of exponential fits to transverse mass distributions.

Target	p (GeV/c)	C_0 (GeV$^{-2}c^2$)	T (MeV/c)
Au	17.5	$(4.90\pm0.62)\times10^{-4}$	157 ± 34
Au	12.3	$(1.85\pm0.91)\times10^{-4}$	98 ± 58
Cu	12.3	$(2.84\pm0.95)\times10^{-4}$	108 ± 47
Be	12.3	$(4.10\pm0.92)\times10^{-4}$	86 ± 19

ferent beam energies, such behavior is consistent with more reabsorption in a larger target. The beam energy dependence of $\langle p_T \rangle$, as previously measured in $p+p$ collisions [15], cannot solely account for the observed difference in slope.

The yields tend to increase with decreasing target size. This trend is more evident when the yields are integrated over the entire range of measured y (1–2) and p_T (10–800 MeV/c). These yields, dn/dy with $y=1$–2 and integrated over p_T, are shown in Fig. 3. There is a $(34\pm22)\%$ decrease in dn/dy from the Be target to the Au target. The 17.5 GeV/c $p+$Au yield is shown in the same figure for comparison. The yield from $p+$Au at 17.5 GeV/c is 3.1 times the yield at 12.3 GeV/c. Although the likelihood of producing antiprotons may be greater in a larger nucleus [16], the likelihood of reabsorption is also greater due to the presence of more baryons. At these beam energies, we find the effect of increased reabsorption in the larger nucleus to be greater than any possible increase in production.

The dependence of the yields on the beam momentum can be described by the available kinetic energy squared. It was shown [17] that antiproton yields for $p+p$ collisions at energies near the production threshold can be described by

$$(\text{KE})^2 = (\sqrt{s} - 4m)^2, \tag{2}$$

where m is the mass of the antiproton. In the reference, it is also shown (using phase-space arguments) that this dependence can be explained by production through a three-body process rather than a four-body process, indicating the possibility of an intermediate state. Figure 4 shows that this dependence also describes well our $p+$Au yields. Having established this dependence, we can compare to data at a different beam energy.

Figure 5 shows a comparison between our measurement of dn/dy and the measurement by E802 [18]. For the purpose of direct comparison, we have restricted our y range
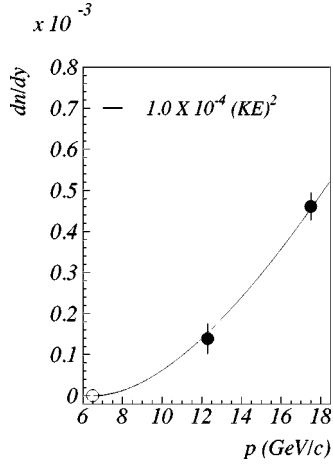
FIG. 4. Energy dependence of E910 $p+$Au $\bar{p}$ yields; $\bar{p}$ yields vs beam momentum ($\bullet$); $\bar{p}$ production threshold ($\bigcirc$). The curve shows yields follow a $(KE)^2$ dependence.

from 1 to 1.6 and scaled the yields using $(KE)^2$ to correspond to the 14.6 GeV/c beam momentum of E802. Although the measurements are consistent with each other, E802 concluded no target dependence. With increased statistics and a larger range in y (Fig. 3), we conclude that there is indeed a modest target dependence at AGS energies.

In addition to our inclusive measurements for different targets and beam energies, we can use the dependence of the $\bar{p}$ multiplicity on centrality to help disentangle the mechanisms of production and reabsorption in the nucleus. The centrality (or ν) dependence of $\bar{p}$ yields is shown in Fig. 6. The antiproton yields are measured for each value of N_g and then plotted versus the mean ν for a given N_g. Since the
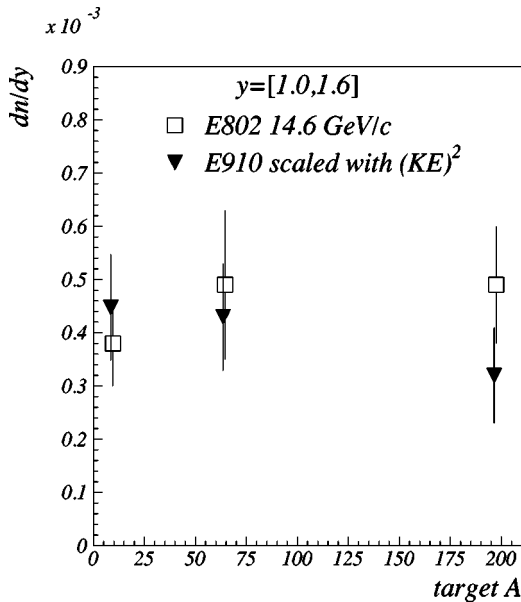

FIG. 5. Comparison between E910 12.3 GeV/c $\bar{p}$ yields ($\blacktriangledown$) extrapolated to 14.6 GeV/c and E802 measurements ($\square$). See text for details. The points from the two experiments are offset relative to each other in order to distinguish the error bars.
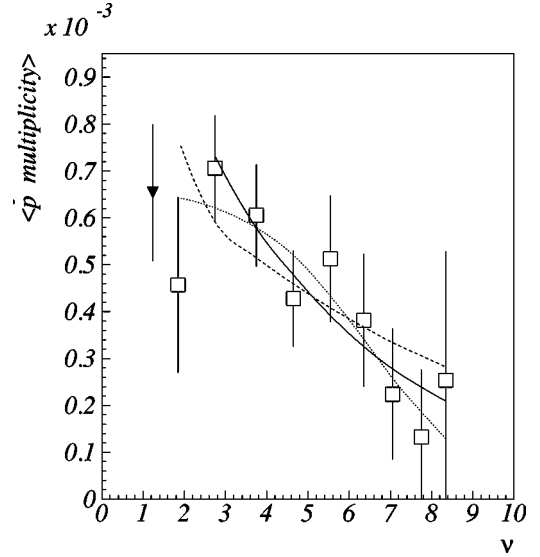

FIG. 6. Dependence of 17.5 GeV/c $p+$Au $\bar{p}$ yields on $\langle \nu(N_g) \rangle$ ($\square$). Lines show results of absorption fits. Fit 1 is shown by the dashed curve, fit 3 the dotted curve, and fit 4 the solid curve (see Table III for details). Also shown is 12.3 GeV/c $p+$Be data point extrapolated to 17.5 GeV/c ($\blacktriangledown$).

$N_g=0$ bin corresponds to a mean of approximately two projectile collisions for $p+$Au, we have plotted the first N_g bin for $p+$Be on the same figure (scaled from 12.3 to 17.5 GeV/c beam momentum using the $(KE)^2$ relationship discussed above) simply as a reference of what the production may be in only one $p+N$ collision. Although we may be somewhat biased against antiproton production in the $N_g=0$ bin (the antiproton may be preferentially produced together with a slow proton due to baryon number conservation), it is possible that the increase from $N_g=0$ to $N_g=1$ is due to contributions to production beyond the first $p+N$ collision. However, with the exception of the yield in the first $p+$Au N_g bin to the second, we see the mean antiproton multiplicity decrease as the number of projectile collisions increases. This relationship gives insight to the amount of nuclear material traversed by the antiproton before it is reabsorbed. With a few phenomenological assumptions, we present a quantitative measure of the survival probability of an antiproton as a function of the amount of nuclear material through which it passes. Because the beam energy is close to production threshold and the antiprotons are strongly peaked at forward angles, we assume that only the first collisions contribute to the production of antiprotons, which are then assumed to follow the path of the projectile through the nucleus. Since we have conjectured possible contributions to production beyond the first collision, we will discuss the effect of such a modification to our assumptions later in the text. With this picture of $\bar{p}$ production, we quantify the reabsorption with the following equation,

$$\sigma(pA \rightarrow \bar{p}X) = \sigma(pp \rightarrow \bar{p}X)e^{-(\sigma_{abs}/\sigma_{pN})(\nu-1)}, \qquad (3)$$

where $\sigma(pp \rightarrow \bar{p}X)$ is the antiproton production cross section for $p+p$, σ_{abs} is the "effective" antiproton absorption cross

TABLE III. Fit parameters of antiproton absorption fits. Fits 1–3 include the first $p+$ Au data point in the fit, and fits 4–6 do not.

Fit	σ_{abs} (mb)	τ_{form} (fm/c)	Constraint	χ^2/No. degrees of freedom
1	4.0 ± 1.6	0	$\tau_{form}=0$	6.994/7
2	4.2 ± 1.6	1	$\tau_{form}=1$	6.562/7
3	38	4.9 ± 0.5	$\sigma_{abs}=38$	3.149/7
4	6.9 ± 2.2	0	$\tau_{form}=0$	2.005/6
5	6.9 ± 2.4	1	$\tau_{form}=1$	1.995/6
6	38	4.7 ± 0.7	$\sigma_{abs}=38$	1.928/6

section, and σ_{pN} is the proton-nucleon interaction cross section. Since the "ν" plotted on the x axis of Fig. 6 is simply an average value, $\bar{\nu}(N_g)$, and each value of N_g actually has a distribution of ν values associated with it, $P_{N_g}(\nu)$, we fold the above exponential with $P_{N_g}(\nu)$. We determine σ_{abs} by fitting the ν-dependent antiproton yields with the following function:

$$\sigma(pA\rightarrow\bar{p}X)=\sigma(pp\rightarrow\bar{p}X)P_{N_g}(\nu)e^{-(\sigma_{\mathrm{abs}}/\sigma_{pN})(\nu-1)}. \quad (4)$$

Folding the distribution, $P_{N_g}(\nu)$, for discretized values of N_g results in a steplike behavior of the fit. We show smoothed fit functions in the figure. The results of the fits with various sets of assumptions are shown in Table III. We have done the fits with and without allowing for a formation time,

$$\tau_{\mathrm{form}}=\frac{\nu_{\mathrm{form}}\lambda}{\gamma\upsilon}, \quad (5)$$

during which the antiproton cannot annihilate. In this case, the exponent in Eq. (4) becomes $-(\sigma_{\mathrm{abs}}/\sigma_{pN})(\nu-\nu_{\mathrm{form}}-1)$ for $\nu>\nu_{\mathrm{form}}+1$, and there is no absorption ($\sigma_{\mathrm{abs}}=0$) for $\nu\leq\nu_{\mathrm{form}}+1$. One should note that the linear relationship between ν_{form} and τ_{form} is not as straightforward for very large values of ν_{form}, which rely on fluctuations in the nuclear density distribution. The quantities that are used to calculate σ_{abs} and τ_{form} from the fit parameters are a mean free path λ of 2 fm and a proton-nucleon interaction cross section σ_{pN} of 30 mb. Using a momentum of 2.5 GeV/c (the mean measured momentum for the antiprotons we detect), we calculate γ and υ. In the first three fits shown in the table, we include the first $p+$ Au data point ($N_g=0$) in the fit, and in the next set of three fits, we do not include this point (because of the initial increase in yield from $N_g=0$ to $N_g=1$). In addition to removing a possible bias in the first data point from the fit, this also allows for production beyond the first collision up to the value of $\nu=2.4$ where the fit begins.

The first row shown in Table III is the result of a fit assuming that the formation time is negligible. Given that the free annihilation cross section σ_{ann} is 38 mb at a momentum of 2.5 GeV/c, the extracted σ_{abs} is significantly reduced relative to σ_{ann} (almost by a factor of 10). This fit is shown in Fig. 6 as a dashed curve. In the following two fits, we investigate the effect of a formation time τ_{form} on this result. With no constraints on the fit, τ_{form} is very large. However, with

excessively large τ_{form} we lose the ability to uniquely determine σ_{abs} from the fit. Thus, we constrain τ_{form} and σ_{abs} separately in 2 fits. Typical values used in transport models for the formation time are 1–2 fm/c [19]. Constraining τ_{form} to such values results again in a reduced absorption cross section. The fit parameters shown in fit 2 in the table are for a constraint of $\tau_{\mathrm{form}}=1$ fm/c, with which one obtains a $\sigma_{\mathrm{abs}}=4.2\pm1.6$ mb. (This fit looks similar to the fit with no formation time and is, therefore, not shown in the figure.) The other possibility is to constrain the absorption cross section to be equal to the free annihilation cross section, $\sigma_{\mathrm{abs}}=38$ mb. Such a constraint leads to $\nu_{\mathrm{form}}=6.7\pm0.7$, which corresponds to a long formation time of 4.9 ± 0.5 fm/c or a formation length of approximately 13 fm in the nuclear rest frame. Again, such large values of ν_{form} rely on density fluctuations and thus do not have such a well-defined relationship to τ_{form}. The fit is shown by the dotted curve in Fig. 6. The next three rows repeat the three fits described above, excluding the first $p+$ Au data point from the fit. The results are qualitatively similar to those when including the first data point. Fit 4 in the table, which is shown with a solid curve in the figure, again assumes no formation time and results in a reduced absorption cross section (approximately 5 times smaller than σ_{ann}). When including a formation time of 1 fm/c, fit 5 in the table, σ_{abs} is still reduced by approximately a factor of 5. Finally, fit 6 shows that constraining $\sigma_{\mathrm{abs}}=\sigma_{\mathrm{ann}}$ results in a long formation time, even when excluding the first data point. The large discrepancy between σ_{abs} and σ_{ann}, as derived from our simple model when the formation time is negligible or small (1 fm/c), suggests that the "effective" annihilation cross section is very different from the free annihilation cross section due to in-medium effects. On the other hand, the data can be described by the free p-$\bar{p}$ annihilation cross section and a very long formation time. A possible explanation for such a result is the formation of an intermediate state where τ_{form} can be interpreted as the mean lifetime of the state. With such a large τ_{form}, the antiproton is born only in the late stage of the propagation of this state through the nucleus, leaving little opportunity to get reabsorbed. This hypothesis could be tested by measuring the absorption of other antibaryons which could proceed through the same intermediate state.

In conclusion, we find the yields dramatically increase with increasing beam energy and can be described by a dependence on the available kinetic energy squared. The observed energy dependence can be understood if the antiproton is produced through the decay of an intermediate state [17]. We find a moderate decrease with increasing target mass, $(34\pm22)\%$ from Be to Au for beam momentum 12.3 GeV/c. Finally, we have quantified the survival probability of an antiproton in the nuclear medium as a function of the number of collisions. With this relationship and the assumption of a negligible or small formation time of 1 fm/c, we find that the annihilation cross section is greatly modified within the nuclear medium, and that the "effective" absorption cross section is a small fraction of the free annihilation cross section. On the other hand, a full p-$\bar{p}$ annihilation cross section would require a much longer formation time than

normally assumed. A similar conclusion of a longer formation time for protons than for pions has recently been made by the HERMES collaboration [20]. Previous attempts to explain a suppression of the annihilation of antiprotons within the nucleus include an increased hadron formation time [8,21], the formation of a p-$\bar{p}$ molecule [12,13] with a finite lifetime, and a ''shielding'' effect due to the presence of mesons [11]. All of such phenomenological arguments manifest themselves as a delay time during which the antibaryon cannot annihilate with a baryon. Shielding, in particular, is dependent on the density of the nuclear medium and would probably not be a large effect in proton-nucleus collisions. Our ν-dependent yields, however, show that the reabsorption of antiprotons is already greatly suppressed in $p+A$ collisions. Production through an intermediate state, which does not get absorbed like an antiproton, could also explain a suppression of the annihilation of antiprotons. In conclusion, we observe a deviation from the expectations of the naive first-collision model in which the antiproton is produced on-shell in the first collision with a small or negligible formation time and then interacts with nucleons according to the free p-$\bar{p}$ annihilation cross section.

[1] V. Koch, G. Brown, and C. Ko, Phys. Lett. B **265**, 29 (1991).
[2] C. Spieles *et al.*, Phys. Rev. C **53**, 2011 (1996).
[3] I. Bearden *et al.*, Phys. Rev. C **57**, 837 (1998).
[4] T. Armstrong *et al.*, Phys. Rev. Lett. **79**, 3351 (1997).
[5] R. Rapp and E. Shuryak, Phys. Rev. Lett. **86**, 2980 (2001).
[6] U. Heinz *et al.*, J. Phys. G **12**, 1237 (1986).
[7] S. Gavin *et al.*, Phys. Lett. B **234**, 175 (1990).
[8] J. Costales, Ph.D. thesis, Massachusetts Institute of Technology, 1990.
[9] M. Bennett *et al.*, Phys. Rev. C **56**, 1521 (1997).
[10] A. Jahns *et al.*, Phys. Rev. Lett. **68**, 2895 (1992).
[11] S. Kahana *et al.*, Phys. Rev. C **47**, 1356 (1993).
[12] J. Nagle, Ph.D. thesis, Yale University, 1997.
[13] H. Sorge, J. Nagle, and S. Kumar, Yale Report No. 40609-1233.
[14] I. Chemakin *et al.*, Phys. Rev. C **60**, 024 902 (1999).
[15] A. Rossi *et al.*, Nucl. Phys. B **84**, 269 (1975).
[16] P. Koch and C. Dover, Phys. Rev. C **40**, 145 (1989).
[17] P. Stankus, Ph.D. thesis, Columbia University, 1993.
[18] T. Abbott *et al.*, Phys. Rev. C **47**, 1351 (1993).
[19] S. Bass *et al.*, Prog. Part. Nucl. Phys. **41**, 225 (1998).
[20] A. Airapetian *et al.,* Eur. Phys. J. C (to be published).
[21] A. Vaisenberg *et al.*, Pis'ma Zh. Eksp. Teor. Fiz. **29**, 719 (1979).